

# RadarLLM: Adapting Pretrained Large Language Models for Marine Radar Target Detection with Preference-aware Loss

Qiying Hu

**Abstract**—Recent advances in pre-trained large language models (LLMs) have demonstrated their capacities to capture universal knowledge, making them promising general-purpose optimization solvers for wireless signal processing. Motivated by these findings, we take the first step towards fine-tuning pre-trained LLMs for the effective analysis of radar signal features in marine target detection tasks. Nevertheless, directly fine-tuning pre-trained LLMs on marine target detection tasks tends to suffer from pronounced overfitting, particularly in challenging low signal-to-clutter ratio (SCR) scenarios. This overfitting primarily stems from the model’s tendency to memorize spurious or noisy feature patterns rather than learning discriminative structures that generalize well to unseen data. To address this challenge, we introduce RadarLLM, a novel fine-tuning framework that utilizes an effective preference-aware loss. Unlike conventional training strategies that uniformly optimize all feature tokens, this loss function selectively optimizes different feature patches based on their online evaluated learning values, thus guiding the model to focus on the most generalizable patterns during optimization. We theoretically demonstrate the effectiveness of the evaluated learning values by transforming the problem as selecting useful feature tokens. Extensive experiments on real-world marine radar datasets show that 1) the proposed loss function is much better than the original one, with particularly significant gains in challenging low SCR scenarios and 2) RadarLLM consistently outperforms state-of-the-art baselines across diverse detection scenarios, with particularly notable gains under limited training data conditions.

**Index Terms**—Marine small target detection, radar signal processing, pre-trained large language models (LLMs), preference-aware loss.

## I. INTRODUCTION

WITH the growth of global economic integration, maritime transportation has become crucial for international trade and security. Real-time and precise detection of maritime targets is essential for intelligent monitoring systems and various applications such as search and rescue, environmental monitoring, and national security. Radar technology, known for its ability to operate under diverse weather conditions and around the clock, plays a key role in maritime target detection. However, radar systems are challenged by sea clutter, which significantly obscures small targets and complicates detection. The complex nature of sea clutter makes it difficult to distinguish weak targets from sea clutter, posing a persistent challenge in radar target detection. Detecting small maritime targets, including small boats, frogmen, and fairway buoys,

remains an active research area, as these targets have small radar cross sections and are difficult to identify in cluttered environments.

The early methods for detecting marine targets are typically developed based on the fundamental concept of constant false alarm rate (CFAR), with specific implementations such as CA-CFAR and GO-CFAR. These methods operate by estimating clutter statistics from reference cells to dynamically adjust detection thresholds. Although computationally efficient, these methods exhibit significant limitations in complex marine environments. Empirical studies reveal that their actual false alarm rates (FAR) often deviate drastically from preset parameters, sometimes exceeding theoretical values by orders of magnitude. This inadequacy stems from their reliance on simplistic statistical assumptions, which fail to hold in heterogeneous sea clutter scenarios characterized by spatially varying distributions and nonstationary behaviors. With the development of modern radars with high range and velocity resolution, approaches leveraging multi-domain features of radar echoes have gained significant attention, utilizing phase, Doppler, and time-frequency domain characteristics to distinguish targets from sea clutter. Many researchers have actively engaged in developing approaches that utilize hand-crafted features and machine learning classifiers [1], [2], [3], [4], [5], [6]. However, these methods rely heavily on domain expertise and hand-crafted heuristics, often struggling to capture high-dimensional and complex patterns in the signal feature.

With the rapid development of deep learning technology, deep learning (DL) and neural networks (NN) have gained huge popularity in the computer vision (CV) society and natural language processing (NLP) society. Moreover, DL and NN approaches are also introduced for small marine target detection. These methods primarily utilize radar signal features to train deep neural networks, eliminating the need for precise mathematical models of clutter and targets. As a result, they somewhat reduce the impact of complex environmental conditions on target detection performance by learning to extract meaningful and distinctive features in a high-dimensional space. Some studies use convolutional neural networks (CNNs) [7], [8], [9], [10], [11], [12], [13], recurrent neural networks (RNNs) [14], and graph neural networks (GNNs) [15], [16], [17]. Among all the methods mentioned above, detectors based on sequence features and RNNs [14] or CNNs [10] offer an excellent trade-off between inference speed and detection performance.

Despite recent progress, compact NN models with small pa-

Qiying Hu (huqiyinguestc@hotmail.com)

This work is a preprint and has not undergone peer review. The version presented here may differ from the final published version.

parameter scales and randomly initialized weights often exhibit limited learning capabilities and unstable training processes. These limitations lead to poor detection performance, particularly in scenarios with scarce training data or with significant environmental variability. Extensive recent studies [18], [19], [20], [21], [22], [23], [24] have shown that pre-trained LLM can be a good starting point for wireless signal and time series modeling, as they are pre-trained on massive sequential datasets. Compared to random initialized weights of small models, this starting point may significantly improve model optimization stability and effectiveness. Moreover, the self-attention mechanism in LLM exhibits structural similarity to Principal Component Analysis (PCA) [18], demonstrating strong generality in extracting key features from high-dimensional sequence data. This insight opens a very promising direction for radar target detection by fine-tuning pre-trained LLMs, offering the potential for performance improvements.

Our preliminary study [25] shows that fine-tuning a pre-trained GPT2 model to analyze sequence features yields state-of-the-art detection performance. Extensive ablation experiments further confirm that removing the GPT2 model or substituting it with a randomly initialized Transformer encoder significantly degrades the detection rate.

Although powerful and promising, some challenges still exist. First, the large scale of LLM requires lightweight and efficient fine-tuning strategies, which are essential for practical deployment, especially in resource-constrained settings. Second, and more critically, for radar applications, adapting LLMs to process sequence features in low signal-to-clutter ratio (SCR) conditions is far from a routine task, often leading to severe overfitting issues. This phenomenon is fundamentally attributed to the intrinsic characteristics of sequence features:

- **Significant Clutter-Induced Noise:** In low SCR environments, small targets are frequently obscured by ocean waves. This causes large noise in sequence features, especially in phase and amplitude features, increasing the likelihood of the model overfitting to irrelevant and noisy information.
- **Feature Pattern Convergence Imbalance:** Various patterns in different sequence features often exhibit different convergence rates during fine-tuning. For example, simple and regular patterns may rapidly reach convergence during model training, and then exhibit a tendency for overfitting, whereas other valuable patterns may require more iterations to achieve convergence.

To address the aforementioned challenges, this paper introduces RadarLLM, an innovative framework for learning from radar echo signals. First, we extract five sequence features from radar echo signals and patch them into multiple feature tokens. Second, we train a small reference model based on the validation samples and calculate the loss for each feature token of the training samples to estimate its generalization potential. Third, we construct a target detector based on a pre-trained LLM, then fine-tune the model based on low-rank adaptation (LoRA) [26] and a novel preference-aware loss function, which is inspired by the work in NLP [27] and CV [28].

This loss introduces a selective training strategy by assigning training weights to different feature patches according to their learning values, which greatly improving model performance in low SCR environments. Finally, we retrain a classification head to enhance detection performance and control the false alarm rate.

Here we summarize our key contributions as follows:

- 1) We propose RadarLLM, a novel framework combining a lightweight reference model and a pre-trained LLM for marine radar target detection. To the best of our knowledge, we are the first to show that well-known LLM can be a strong starting point for intelligent radar signal processing.
- 2) For fine-tuning of the framework, we propose a novel preference-aware loss function which greatly improves RadarLLM's performance in a low SCR environment. RadarLLM can selectively optimize on useful feature tokens with high learning values while reducing the risk of overfitting.
- 3) Our extensive experiments confirm the effectiveness of RadarLLM. It attains new state-of-the-art detection performance under sufficient training data, and constrained training data settings on popular marine radar datasets.

The remainder of this paper is structured as follows. Section II briefly summarizes the related work. Section III presents the detailed operating procedure of the proposed RadarLLM. Section IV introduces the experimental results and analysis. Section V concludes our work.

## II. RELATED WORK

### A. Deep Learning Powered Marine Radar Target Detection

Deep learning models with elaborately crafted architectures have demonstrated great promise in marine target detection. Among them, Chen *et al.* [7] design a dual-channel CNN (DCCNN)-based structure detector that extracts both amplitude and time-frequency information from signals to achieve target detection. Qu *et al.* [8] introduce a CNN architecture augmented with asymmetric convolution layers to capture deep features of the time-frequency distribution. Xu *et al.* [9] propose a target detector in the case of limited training samples, utilizing pre-trained CNN to extract features from time-frequency spectrogram. Wan *et al.* [14] propose a sequence-based target detection framework that leverages instantaneous phase, Doppler spectrum, and short-time Fourier transform features, in conjunction with a bidirectional long short-term memory (Bi-LSTM) network. Wang *et al.* [11] propose a target detector based on complex value U-Net (CV-UNet), which realizes clutter suppression based on the amplitude-phase characteristics of radar echoes, and then achieves target detection. Su *et al.* [17] introduce a graph neural network (GNN) approach for radar target detection, which constructs spatio-temporal adjacency matrices, extracts hierarchical features through convolutional graph operations, and outputs detection results via nonlinear vertex embeddings.

In addition to traditional supervised learning, semi-supervised, unsupervised, and incremental learning approaches are proposed to further advance radar target detection. Wang

*et al.* [29] propose a self-evolving framework for maritime radar target detection using semi-supervised learning, which enhances detection performance through unsupervised sample selection, data augmentation, and model optimization. Xia *et al.* [10] introduce an unsupervised contrastive learning framework that learns discriminative representations between targets and clutter from unlabeled data. Wang *et al.* [30] propose an incremental learning-based target detection method, which can continuously adapt the NN model in real time according to environmental changes. These methods provide compelling evidence that deep learning can significantly enhance detection performance without the need for explicit mathematical modeling. However, it is important to recognize certain limitations inherent in these methods. Current methods rely on relatively small NN models, which possess limited feature recognition capabilities and are highly sensitive to environmental variations.

### B. Language Model Powered Signal Processing Task

Recently, LLMs such as ChatGPT and DeepSeek have demonstrated exceptional capabilities in natural language understanding, code generation, math problem solving, and human-like text generation [31]. Some studies also demonstrate their potential in the signal processing (SP) task. For example, Zhou *et al.* [18] propose a unified time series analysis framework by fine-tuning frozen GPT2 [32] and achieving SOTA performance on various datasets. Liu *et al.* [24] propose a GPT2-empowered channel prediction framework to improve prediction accuracy. Sheng *et al.* [33] utilize the GPT2 model to develop an effective and robust beam prediction method. Zheng and Dai [21] propose a multi-task LLM framework to satisfy the requirements of different wireless communication tasks. IOT-LLM and Penetrative AI [34], [35] directly utilize raw signal data as input and chain of thought prompts for reasoning on the Internet of Things (IOT) tasks. However, recent studies [36] have raised concerns about the universal applicability of LLM in signal processing tasks. LLM-based approaches do not always deliver significant performance improvements, implying that their pre-trained parameters sometimes fail to transfer to downstream tasks. In marine radar target detection under low SCR conditions, directly fine-tuning a pre-trained LLM often leads to severe overfitting issues, limiting its parameter transfer capability. We counteract this shortfall with a preference-aware loss through selectively training on useful feature patches.

## III. PROPOSED METHOD

### A. Overview of the RadarLLM Framework

In this study, we present RadarLLM, a LLM-empowered framework for marine radar target detection. The framework introduces a selective patch-level fine-tuning strategy that counteracts the severe overfitting problem caused by the low SCR environment. The overall pipeline of RadarLLM is illustrated in Fig. 1 and shown in Algorithm 1.

First, five complementary sequence features are extracted from radar echoes and partitioned into uniform patches to form a multi-patch representation. Next, a lightweight reference

---

### Algorithm 1 RadarLLM

---

#### Require:

Radar echo signals  $\{x(n)\}_{n=1}^N$  and Target labels  $\{y_b\}_{b=1}^B$   
 Pre-trained LLM parameters  $\theta_{\text{LLM}}$

#### 1: Stage 1: Sequence Feature Extraction

- 1) Extract IP, DSE, SMS, Amp, and DP features from the observation vector, respectively, see Eq.(3), (4), (5),(7), and (9).
- 2) Patch the five features into feature tokens, see Fig. 3.

#### 2: Stage 2: Reference Model Training

- 1) Train a lightweight reference model  $\theta_r$  based on validation samples and CE loss.
- 2) Compute the loss for each feature token of the training samples based on the predicted output probabilities of reference model, see Eq.(20).

#### 3: Stage 3: Fine-tune LLM for Target Detection

- 1) Compute the loss for each feature token of the training samples based on the predicted output probabilities of current model, see Eq.(21).
- 2) Fine-tune LLM for target detection via preference-aware loss function, see Eq.(22) and Eq.(24).

#### 4: Stage 4: Classification Head Retraining

- 1) Train autoencoder classification head based on the weighted sum of reconstruction loss and CE loss, see Eq.(30), Eq.(31), and Eq.(32).
- 2) Adjust detection threshold  $\eta$  for controllable FAR, see Eq.(33).

#### Ensure:

Fine-tuned RadarLLM model with controllable FAR.

---

model rapidly scores each patch to quantify its generalization potential. Then, we fine-tune a pre-trained LLM backbone via a preference-aware loss and Low-Rank Adaptation (LoRA). Finally, an autoencoder-based classification head is re-trained to enhance detection performance and control the false alarm rate. The detailed design and rationale of each module are elaborated in the following subsections.

### B. Stage 1: Sequence Feature Extraction

When the radar transmits coherent pulses toward the sea surface, it receives a sequence of echo signals from each range resolution cell. In clutter-dominated cells, these echoes primarily consist of sea surface backscatter and thermal noise, whereas in target-present cells, additional reflections from the target are superimposed. The received echo sequence  $x$  from a resolution unit can be decomposed into observation vectors  $x_i$  through the following segmentation:

$$x_i = [x(M \cdot (i - 1) + m)]_{m=1}^N, \quad i = 1, 2, \dots \quad (1)$$

where  $N$  represents the length of the observation window and  $M$  denotes the sliding step between consecutive observation vectors. Target detection is formulated as a binary hypothesis

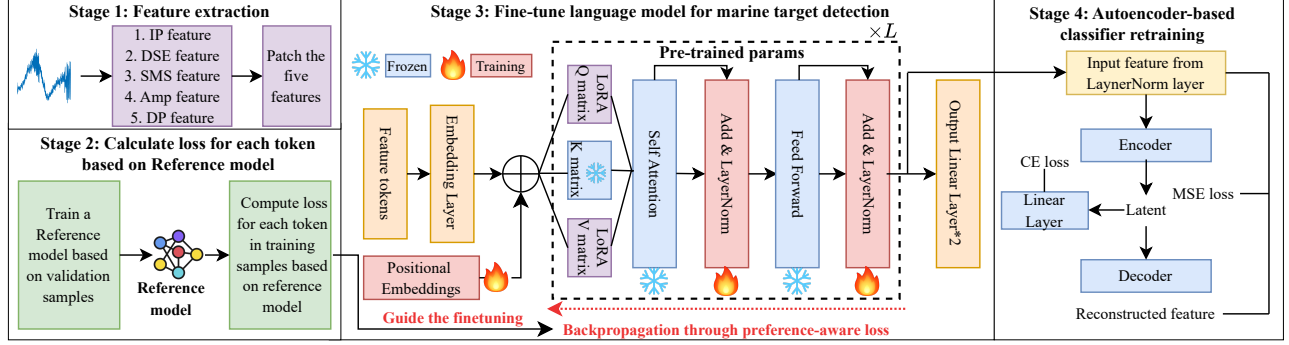


Fig. 1. Overview of our RadarLLM framework.

testing problem:

$$\begin{cases} H_0 : \begin{cases} x(n) = c(n), & n = 1, 2, \dots, N \\ x_p(n) = c_p(n), & p = 1, 2, \dots, P \end{cases} \\ H_1 : \begin{cases} x(n) = s(n) + c(n), & n = 1, 2, \dots, N \\ x_p(n) = c_p(n), & p = 1, 2, \dots, P \end{cases} \end{cases} \quad (2)$$

where  $H_0$  is the null hypothesis that indicates target absence in received signal  $x(n)$ , and  $H_1$  is the alternative hypothesis that indicates target presence. In the cell under test,  $s(n)$  and  $c(n)$  denote target echos and sea clutter echos, respectively. Meanwhile, in the reference cells,  $x_p(n)$  and  $c_p(n)$  denote received echos and clutter echos, respectively.  $P$  is the number of reference cells. To effectively distinguish between the target echo and clutter echo, five unique sequence features are extracted from the time, phase, Doppler, and time frequency domains, as described below:

- Instantaneous Phase (IP): The instantaneous phase of the radar echo signal  $x(n)$  is calculated as follow:

$$\phi(n) = \arg[x(n)], \quad (3)$$

where  $\arg(\cdot)$  represents the phase of a complex variable.

- Doppler Spectrum Entropy (DSE): For the echo signal  $x(n)$ , its Doppler amplitude spectrum can be represented as:

$$F(f_d) = \frac{1}{\sqrt{N}} \left| \sum_{n=0}^{N-1} x(n) \exp(-j2\pi f_d n T_s) \right|, \quad (4)$$

where  $f_d(-\frac{1}{2T_s} \leq f_d \leq \frac{1}{2T_s})$  represents the Doppler frequency, and  $T_s$  represents the pulse repetition interval for the radar system. Furthermore, the entropy of the Doppler spectrum is calculated as:

$$\text{DSE}(F) = -\tilde{F}(f_d) \log \tilde{F}(f_d), \quad (5)$$

where  $\tilde{F}(f_d) = \frac{F(f_d)}{\sum_{f_d} F(f_d)}$ .

- Short-Time Fourier Transform Magnitude Spectrum (SMS): Due to the non-stationary characteristics of the radar echo signal, short-time fourier transform (STFT) provides a more comprehensive understanding compared to Doppler transform, which is calculated as:

$$S(k, m) = \sum_{n=-\infty}^{\infty} x(n) w(n-m) e^{-j2\pi \frac{kn}{\Omega}}, \quad (6)$$

where  $w(\cdot)$  is the window function,  $\Omega$  is the number of frequency bins,  $m$  represents the time index, and  $k$  is the frequency index. To make the features suitable for input into a sequence neural network, we compute the time-averaged magnitude of  $S(k, m)$  and convert it into a decibel (dB) scale. Specifically, for each frequency index  $k$ , the following computation is performed:

$$\text{SMS}(k) = 10 \log_{10} \left( \sum_{m=0}^{N-1} |S(k, m)| \right). \quad (7)$$

- Amplitude (Amp): The instantaneous amplitude is computed by calculating the magnitude of the complex radar echo signal:

$$A(n) = |x(n)|. \quad (8)$$

- Doppler Phase (DP): The Doppler phase is extracted from the Doppler transform of echo signal:

$$\text{DP}(f_d) = \arg \left( \sum_{n=0}^{N-1} x(n) \exp(-j2\pi f_d n T_s) \right). \quad (9)$$

As shown in Fig. 2, the five sequence features reveal clear distinctions between target and clutter samples.

### C. Structure of the RadarLLM Network

Initially, for a batch of  $B$  samples, the input feature matrix is constructed by concatenating the IP feature  $F_{\text{IP}}$ , DSE feature  $F_{\text{DSE}}$ , SMS feature  $F_{\text{SMS}}$ , amplitude feature  $F_{\text{Amp}}$ , and DP features  $F_{\text{DP}}$ .

$$F = \text{Concat}(F_{\text{IP}}, F_{\text{DSE}}, F_{\text{SMS}}, F_{\text{Amp}}, F_{\text{DP}}). \quad (10)$$

Each feature in  $F$  is subsequently partitioned into non-overlapping patches of length  $L$ . If the final patch is shorter than  $L$ , zero padding is applied to ensure uniform length. The resulting  $K$  patches are concatenated to construct the final input tensor  $F^{\text{P}} \in \mathbb{R}^{B \times K \times L}$ , where  $K = 5 \lfloor \frac{N}{L} \rfloor$ . An illustration of this patching process is provided in Fig. 3.

To adapt the feature patches to the input format required by the pre-trained language model, we employ a fully connected layer to project  $F^{\text{P}}$  into an embedded representation  $F^{\text{EB}} \in \mathbb{R}^{B \times K \times L'}$ . This is followed by the addition of a positional

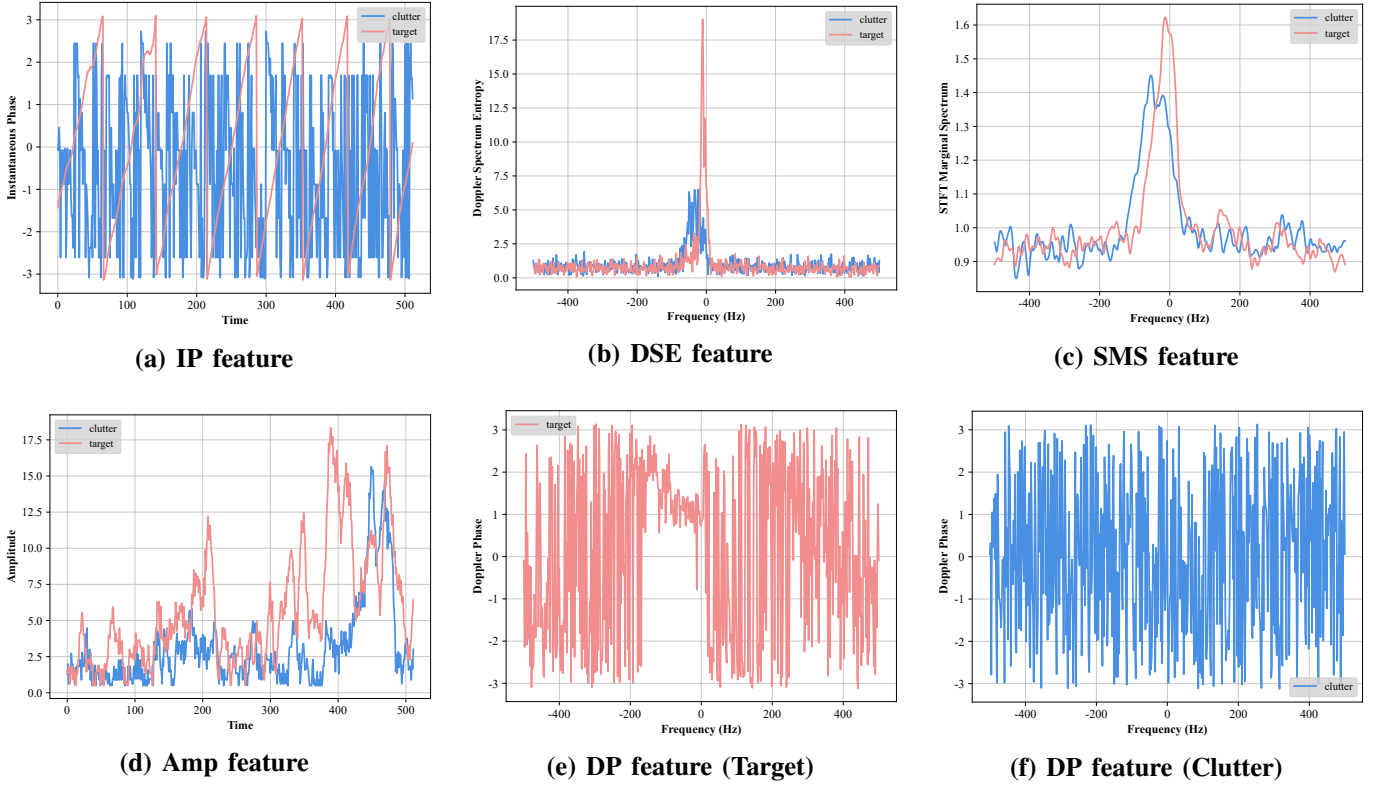


Fig. 2. IP, DSE, SMS, Amp, and DP features for target and sea clutter echo signal on IPIX database.

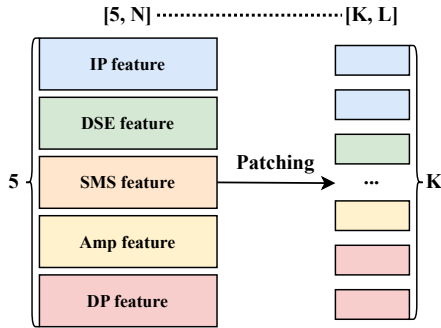


Fig. 3. An illustration of the patching operation.

encoding  $E^{\text{pos}}$ , which incorporates either relative or absolute positional information into the embedded features:

$$E_{b,k,2l}^{\text{pos}} = \sin\left(\frac{k}{10000^{2l/L'}}\right), \quad E_{b,k,2l+1}^{\text{pos}} = \cos\left(\frac{k}{10000^{2l/L'}}\right), \quad (11)$$

where  $b$  represents the  $b$ -th sample,  $k$  represents the position index of the token, and  $l$  denotes the feature dimension index. The positional encoding  $E^{\text{pos}}$  is added to the embedding  $F^{\text{EB}}$  to produce an enriched embedding:

$$F^{\text{PE}} = F^{\text{EB}} + E^{\text{pos}}. \quad (12)$$

The enriched embedding  $F^{\text{PE}}$  is passed through initial several layers of the GPT2 encoder for further feature extraction.

To efficiently fine-tune the backbone model, we apply Low-Rank Adaptation (LoRA) [26] to the query ( $\mathbf{W}_Q$ ) and value matrices ( $\mathbf{W}_V$ ) in the multi-head attention layers and directly fine-tune the Layer Normalization (LayerNorm) parameters. The LoRA fine-tuning process is illustrated in Fig. 4. This strategy introduces lightweight, trainable low-rank matrices to the fixed pre-trained weights, substantially reducing the computational and memory requirements compared to full parameter fine-tuning. Formally, the adapted model generates rich contextual feature representations as follows:

$$F^{\text{LLM}} = \text{LLM}_{\text{LoRA}}(F^{\text{PE}}) \in \mathbb{R}^{B \times K \times L'}, \quad (13)$$

where  $\text{LLM}_{\text{LoRA}}(\cdot)$  represents the backbone network of the language model encoder enhanced with LoRA modules. To stabilize the training process, a Layer Normalization (LayerNorm) operation is applied to the output representation  $F^{\text{LLM}}$ .

$$F^{\text{LN}} = \text{LayerNorm}(F^{\text{LLM}}), \quad (14)$$

where  $\text{LayerNorm}(\cdot)$  is defined element-wise for each position  $k$  and feature dimension  $l$  as:

$$F_{b,k,l}^{\text{LN}} = \gamma_{b,l} \cdot \frac{F_{b,k,l}^{\text{LLM}} - \mu_{b,l}}{\sqrt{\sigma_{b,l}^2 + \epsilon}} + \beta_{b,l}, \quad (15)$$

where  $\mu_{b,l}$  and  $\sigma_{b,l}^2$  is computed as:

$$\mu_{b,l} = \frac{1}{K} \sum_{k=1}^K F_{b,k,l}^{\text{LLM}}, \quad \sigma_{b,l}^2 = \frac{1}{K} \sum_{k=1}^K (F_{b,k,l}^{\text{LLM}} - \mu_{b,l})^2. \quad (16)$$

Here,  $\gamma_{b,l}$  and  $\beta_{b,l}$  are learnable parameters, and  $\epsilon$  is a small constant for numerical stability.  $F^{\text{LN}}$  are then passed through two FC layers to obtain the final output:

$$F^{\text{fi}} = FC(FC(F^{\text{LLM}})) \in \mathbb{R}^{B \times K \times 2}. \quad (17)$$

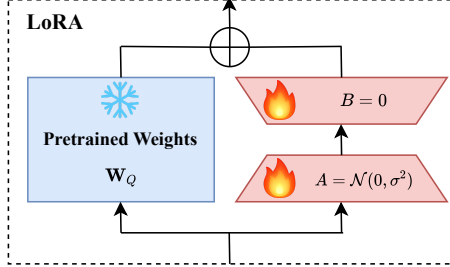


Fig. 4. Illustration of the LoRA fine-tuning process.

#### D. Stage 2: Compute Loss for Each Token Based on the Reference Model

The architecture of the reference model is illustrated in Fig. 5. As described in Section III-C, the input patches are first projected into a latent Transformer space of dimension  $D$  and augmented with learnable additive positional embeddings. This process yields the enriched representation  $F^{\text{PE}'} \in \mathbb{R}^{B \times K \times D}$ , which is subsequently processed by a Transformer encoder. Within the encoder, the multi-head attention (MHA) mechanism functions as follows: the input  $F^{\text{PE}'}$  is linearly projected into  $H$  independent attention heads. For each head  $h$ , query, key, and value matrices  $\mathbf{W}_{Q_h} \in \mathbb{R}^{B \times D \times d_k}$ ,  $\mathbf{W}_{K_h} \in \mathbb{R}^{B \times D \times d_k}$ ,  $\mathbf{W}_{V_h} \in \mathbb{R}^{B \times D \times d_v}$  are used to compute:

$$\mathbf{Q}_h = F^{\text{PE}'} \mathbf{W}_{Q_h}, \quad \mathbf{K}_h = F^{\text{PE}'} \mathbf{W}_{K_h}, \quad \mathbf{V}_h = F^{\text{PE}'} \mathbf{W}_{V_h}, \quad (18)$$

where  $d_k = d_v = D/H$ . The attention output of each head is then computed as:

$$\mathbf{O}_h = \text{Softmax} \left( \frac{\mathbf{Q}_h \mathbf{K}_h^\top}{\sqrt{d_k}} \right) \mathbf{V}_h. \quad (19)$$

Outputs from all heads are concatenated along the feature dimension and projected back to dimension  $D$ . The MHA block further incorporates Batch Normalization layers and a feed-forward network (FFN) equipped with residual connections, resulting in the final encoded representation  $F^{\text{TF}} \in \mathbb{R}^{B \times K \times D}$ . Subsequently, LayerNorm is applied, followed by two fully connected layers to yield the final output  $F^{\text{fi}'} \in \mathbb{R}^{B \times K \times 2}$ .

#### E. Stage 3: Fine-tune RadarLLM Network Based on the Preference-aware Loss

1) *Methodology*: To improve fine-tuning of LLMs for radar target detection in low SCR scenarios, we propose a token-level preference-aware loss function. In such conditions, many feature patches are either severely corrupted by noise or trivially easy, offering limited value for effective learning.

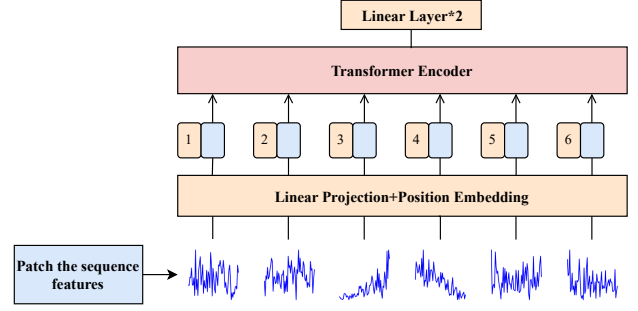


Fig. 5. Overview of the reference model.

Uniformly optimizing all patches risks overfitting by forcing the model to learn from uninformative or misleading inputs. To address this, we introduce a dynamic weighting mechanism that prioritizes tokens with higher learning value, those expected to contribute more to generalization. Specifically, our approach utilizes a dual-model framework consisting of a lightweight reference model  $\theta_r$  and a high-capacity target model  $\theta_t$ , which leverages LLMs.

- **Reference Model:** The reference model is built with a lightweight Transformer encoder and trained solely on validation samples using standard cross-entropy loss. By leveraging the reference model, we can estimate the generalization potential of each feature token in the training samples. A lower reference loss indicates that the token can be effectively captured by a lightweight model, suggesting strong generalization potential. In contrast, a higher reference loss typically reflects excessive noise, making the token less useful for improving detection performance.
- **Target Model:** A significantly larger model built upon a pre-trained LLM, parameterized by  $\theta_t$ , as described in Section III-C.

For a batch of training samples, we compute the token-level cross-entropy losses for both models. Given a feature token  $F_{b,k}^{\text{fi}}$ , the corresponding two losses are as follows:

- **Reference Loss:**

$$\mathcal{L}_{\theta_r, b, k}(F_{b, k}^{\text{fi}}) = - \sum_i y_{b, k}^i \log(\hat{y}_{b, k}^{i, \theta_r}), \quad (20)$$

where  $\hat{y}_{b, k}^{i, \theta_r}$  is the prediction from  $\theta_r$ .

- **Target Loss:**

$$\mathcal{L}_{\theta_t, b, k}(F_{b, k}^{\text{fi}}) = - \sum_i y_{b, k}^i \log(\hat{y}_{b, k}^{i, \theta_t}), \quad (21)$$

where  $\hat{y}_{b, k}^{i, \theta_t}$  is generated by the fine-tuned much larger model  $\theta_t$ .

The core of our method lies in computing a token importance score  $s_{b, k}$  based on the discrepancy between the target loss and reference loss:

$$s_{b, k} = \text{ReLU}(\mathcal{L}_{\theta_t, b, k}(F_{b, k}^{\text{fi}}) - \alpha \mathcal{L}_{\theta_r, b, k}(F_{b, k}^{\text{fi}})), \quad (22)$$

where  $\alpha$  is a scaling coefficient, and  $\text{ReLU}(\cdot)$  ensures that only tokens with positive excess loss are trained. Tokens with low

importance score are not prioritized for optimization because they have already been well learned, as indicated by a low target loss  $\mathcal{L}_{\theta_t, b, k}$ , or with large noise, as reflected by a high reference loss  $\mathcal{L}_{\theta_r, b, k}$ . The  $\text{ReLU}(\cdot)$  function is defined as:

$$\text{ReLU}(x) = \begin{cases} x & x > 0 \\ 0 & x \leq 0 \end{cases} \quad (23)$$

More detailedly, this strategy results in the following selective training scheme:

- If the target loss is much larger than the reference loss, the token is deemed with large learning value, and is therefore prioritized for training.
- If the reference loss is large, the token shows weak generalization potential and a high risk of overfitting; therefore, its training weight is reduced during optimization.
- If the target loss is already small, the token has been sufficiently learned, and further training brings little gain, the training weight is also reduced to avoid redundant updates.

The final training loss is a weighted sum over all feature tokens across the mini-batch, where each token's contribution is scaled by a token-level importance score:

$$\mathcal{L}_{\text{final}} = \frac{1}{B * K} \sum_{b=1}^B \sum_{k=1}^K s_{b,k} \cdot \mathcal{L}_{\theta_t, b, k}(F_{b,k}^{\text{fi}}). \quad (24)$$

where  $B$  and  $K$  denote the batch size and the number of feature tokens, respectively.

2) *Theoretical Insight of the Effectiveness of Feature Token Importance:* We begin by formalizing the task of selecting informative feature patches for training. At each step  $t$ , given a candidate set  $B_t$ , our objective is to select a feature patch  $(F_{b,k}^{\text{fi}}, y_b^k) \in B_t$  whose inclusion in the training set  $D_t$  achieves the maximal reduction in generalization loss on the test set  $D_{\text{te}}$ . This can be formally formulated as the following optimization problem:

$$\arg \min_{(F_{b,k}^{\text{fi}}, y_b^k) \in B_t} -\log p(y^{\text{te}} | F^{\text{te}}; D_t \cup (F_{b,k}^{\text{fi}}, y_b^k)). \quad (25)$$

Directly optimizing Eq.(25) is computationally prohibitive, as it entails retraining the model for each candidate feature patch. To derive a tractable surrogate, we reformulate Eq.(25) using Bayes' theorem:

$$\begin{aligned} & -\log p(y^{\text{te}} | F^{\text{te}}; D_t \cup (F_{b,k}^{\text{fi}}, y_b^k)) \\ &= -\log \frac{p(y, y^{\text{te}} | F, F^{\text{te}}, D_t)}{p(y | F; D_t)}. \end{aligned} \quad (26)$$

Assuming that each label is statistically independent of the other pairs in the corpus when conditioned on its own feature vector, the joint term in the numerator can be expressed as:

$$\begin{aligned} & p(y, y^{\text{te}} | F, F^{\text{te}}, D_t) \\ &= p(y | F; F^{\text{te}}, y^{\text{te}}, D_t) p(y^{\text{te}} | F^{\text{te}}, F, D_t) \\ &= p(y | F; y^{\text{te}}, F^{\text{te}}, D_t) p(y^{\text{te}} | F^{\text{te}}; D_t). \end{aligned} \quad (27)$$

Substituting Eq.(27) into Eq.(26) gives:

$$\begin{aligned} & \log p(y^{\text{te}} | F^{\text{te}}; D_t \cup (F_{b,k}^{\text{fi}}, y_b^k)) \\ &= \log \frac{p(y | F; y^{\text{te}}, F^{\text{te}}, D_t) p(y^{\text{te}} | F^{\text{te}}, D_t)}{p(y | F; D_t)} \\ &\propto \log p(y | F; y^{\text{te}}, F^{\text{te}}, D_t) - \log p(y | F; D_t) \\ &\propto \mathcal{L}[y_b^k | F_{b,k}^{\text{fi}}; D_t] - \mathcal{L}[y_b^k | F_{b,k}^{\text{fi}}; D_t, D_{\text{te}}]. \end{aligned} \quad (28)$$

In summary, for a model trained on  $D_t$ , the process of identifying the feature patch that minimizes the loss on the test samples in Eq.(25) can be approximated by the following objective:

$$\arg \max_{(F_{b,k}^{\text{fi}}, y_b^k) \in B_t} \mathcal{L}[y_b^k | F_{b,k}^{\text{fi}}; D_t] - \mathcal{L}[y_b^k | F_{b,k}^{\text{fi}}; D_t, D_{\text{test}}]. \quad (29)$$

Eq.(29) indicates that feature patches with larger loss differences contribute more significantly to improve the model performance on test set; thus, the loss difference can be interpreted as the learning value of each feature patch. However, since accessing the test set for retraining on  $D_t \cup D_{\text{test}}$  is prohibited and computationally impractical, we approximate the second term using a lightweight reference model trained solely on validation set  $D_{\text{val}}$ . Consequently, the practical token weight is derived as shown in Eq.(22).

#### F. Stage 4: Retrain Classification Head Based on Autoencoder Network

As illustrated in Fig. 1, the output of the LLM-based model has a shape of  $[B, K, 2]$ , representing predictions across multiple tokens. This token-level output cannot be directly used for detection due to the absence of a unified decision representation. To address this, we propose retraining a classifier based on the learned representation  $F^{\text{LN}}$ . Specifically, we employ an autoencoder-based classification head designed to extract the most informative features from the high-dimensional input, thereby enabling effective and robust decision-making. The proposed autoencoder-based classification head comprises three key components: (1) an encoder, consisting of convolutional layers followed by fully connected layers, which extracts compact and discriminative feature representations from  $F^{\text{LN}}$ ; (2) a decoder, symmetrically constructed with convolutional and fully connected layers, which reconstructs the input from the latent space to promote feature consistency and preservation; and (3) a classification head, which operates on the latent vector to perform the final classification. The autoencoder is trained with a dual-objective loss that combines reconstruction loss and classification loss. The reconstruction loss ensures that the latent representation retains critical information by minimizing the discrepancy between the original input  $F^{\text{LN}}$  and its reconstruction  $\hat{F}^{\text{LN}}$ :

$$\mathcal{L}_{\text{recon}} = \left\| F^{\text{LN}} - \hat{F}^{\text{LN}} \right\|_2^2. \quad (30)$$

The classification loss ensures accurate predictions by aligning the predicted probability distribution  $\hat{y}_b^i$  with the ground-truth label  $y_b^i$ .

$$\mathcal{L}_{\text{ce}} = -\frac{1}{B} \sum_{b=1}^B \sum_{i=1}^2 y_b^i \log \hat{y}_b^i. \quad (31)$$

To jointly optimize both the reconstruction and classification objectives, we adopt a task uncertainty weighting strategy [37], which adaptively adjusts the contribution of each loss term based on its inherent uncertainty. The total loss function is expressed as:

$$\mathcal{L}_{\text{total}} = \frac{1}{2\sigma_{\text{recon}}^2} \mathcal{L}_{\text{recon}} + \frac{1}{\sigma_{\text{ce}}^2} \mathcal{L}_{\text{ce}} + \log \sigma_{\text{recon}} \sigma_{\text{ce}}, \quad (32)$$

where  $\sigma_{\text{recon}}$  and  $\sigma_{\text{ce}}$  are learnable parameters representing the task-dependent uncertainties for the reconstruction and classification losses, respectively. This formulation allows the model to balance the learning dynamics of both tasks in a principled and data-driven manner.

To control the false alarm rate during inference, we sort the first element in the softmax output for all test clutter samples in descending order, yielding a one-dimensional array  $O_{\text{sorted}}$ . The detection threshold  $\eta$  is then determined based on the desired false alarm rate  $P_{fa}^d$  as follows:

$$\eta = O_{\text{sorted}}(x), \quad x = \lceil P_{fa}^d \times N_{\text{clutter}} \rceil, \quad (33)$$

where  $O_{\text{sorted}}(x)$  denotes the  $x$ -th largest output in the sorted array,  $N_{\text{clutter}}$  is the total number of test clutter samples, and  $\lceil \cdot \rceil$  is the ceiling operation to ensure integer indexing.

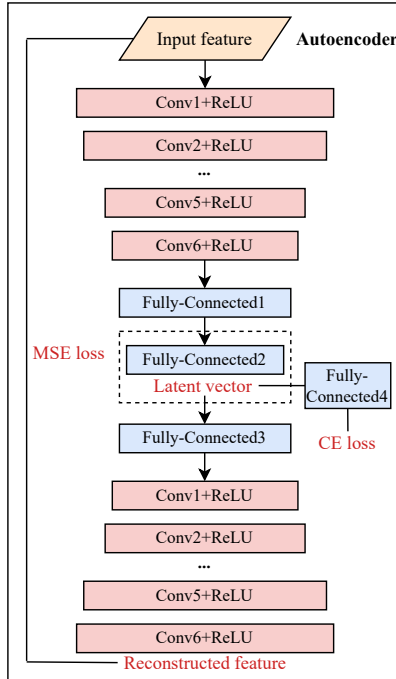


Fig. 6. Overview of the autoencoder model.

#### IV. EXPERIMENTS

In this section, we first describe the experimental setup, followed by a comprehensive evaluation of RadarLLM’s detection performance under three settings: sufficient training data, constrained training data, and zero-shot scenarios.

#### A. Experimental Setup

1) *Dataset*: We employ eight benchmark data sequences (Data1–Data8) from the Intelligent Pixel Processing X-band (IPIX) radar archive, summarized in Table I. All datasets were recorded in 1993 by the IPIX radar on Canada’s east coast and include full polarization measurements (HH, HV, VH, and VV). Each set contains 14 range cells sampled at 1 kHz, with 131 072 complex echoes per cell, yielding an observation window of 0.512 s per sample. Returns from the primary range cell constitute target echoes, whereas returns from the remaining clutter-only cells represent sea clutter. To facilitate performance analysis across varying operating conditions, Data1–Data3 correspond to low signal-to-clutter ratio (SCR) scenes, while Data4–Data8 represent high-SCR scenes.

To ensure sufficient training data, we employ overlapped segmentation following the partition rule in Eq. (1), with parameters set to  $M = 32$  for target cells and  $M = 128$  for clutter cells. This process generates 4,079 target samples and more than 9,000 clutter samples per dataset. The samples are divided into three groups: (1) a training set using the first 20% of observation time for both the target and clutter cells, (2) a validation set covering 20% to 35% of the observation time, and (3) a test set containing the remaining samples.

2) *Baselines*: To validate the superiority of RadarLLM, eight deep learning-based marine radar target detection methods are implemented as baselines. Among them, RNN, Bi-LSTM, GRU, Transformer, PatchTST, and ResNet18 represent lightweight models that utilize sequence features; OFA uses a large language model backbone to process sequence features; and ADN18 utilizes time-frequency maps and enhanced CNNs for detection.

- RNN [14]: RNN is a sequential neural architecture with temporal feedback loops. In experiments, the number of RNN layers and the hidden layer nodes are set to 2 and 6, respectively.
- Bi-LSTM [14]: Bi-LSTM enhances the traditional Long Short-Term Memory (LSTM) by incorporating bidirectional processing. In our implementation, the number of LSTM layers and the number of hidden units per layer are set to 2 and 6, respectively.
- GRU [38]: GRU employs simplified gating mechanisms compared to LSTM. In experiments, the number of GRU layers and the hidden layer nodes are set to 2 and 8, respectively.
- Transformer [39]: Transformer evolutionizes sequence processing through self-attention mechanisms. In experiments, the Transformer encoder is configured with a model dimensionality of 32, comprising 2 layers and 8 attention heads. The feed-forward network (FFN) within each layer is designed with a hidden size of 128.
- PatchTST [40]: PatchTST segments the sequence features into local patches and leverages a Transformer encoder to model them. In experiments, the Transformer encoder is configured with a model dimensionality of 64, comprising 2 layers and 16 attention heads. The feed-forward network (FFN) within each layer is designed with a hidden

TABLE I  
OVERVIEW OF THE IPIX DATABASE.

Label	Name	File name	Primary	Secondary	SCR
1	17	19931107_135603_starea	9	8,10,11	Low
2	25	19931108_213827_starea	7	6,8	Low
3	26	19931108_220902_starea	7	6,8	Low
4	54	19931111_163625_starea	8	7,9,10	High
5	280	19931118_023604_stareC0000	8	7,9,10	High
6	283	19931118_035737_stareC0000	10	8,9,11,12	High
7	311	19931118_162658_stareC0000	7	6,8,9	High
8	320	19931118_174259_stareC0000	7	6,8,9	High

TABLE II  
HYPERPARAMETERS FOR NETWORK TRAINING.

Parameter	Value
Batch size	64
Eval batch size	400
Epochs for LLM fine-tuning	500
Epochs for Autoencoder training	300
Optimizer	Adam (betas=(0.9,0.999))
Learning rate for LLM fine-tuning	0.0001
Learning rate for Autoencoder training	0.00001

TABLE III  
HYPERPARAMETERS FOR AUTOENCODER NETWORK.

Block	Layer	Filter	Stride	Padding	Output
Encoder	Conv1+ReLU	512,1 × 1	1	Same	55 × 768
	Conv2+ReLU	256,1 × 1	1	Same	55 × 256
	Conv3+ReLU	128,1 × 1	1	Same	55 × 128
	Conv4+ReLU	64,1 × 1	1	Same	55 × 64
	Conv5+ReLU	32,1 × 1	1	Same	55 × 32
	Conv6+ReLU	16,1*1	1	Same	55*16
Decoder	Flatten+Fully-Connected1	-	-	-	64
	Fully-Connected2	-	-	-	20
	Fully-Connected3+Reshape	-	-	-	55*16
	Conv1+ReLU	32,1*1	1	1	55*32
	Conv2+ReLU	64,1*1	1	1	55*64
	Conv3+ReLU	128,1*1	1	1	55*128
Classifier	Conv4+ReLU	256,1*1	1	1	55*256
	Conv5+ReLU	512,1*1	1	1	55*512
	Conv6+ReLU	768,1*1	1	1	55*768
Classifier	GeLU+LayerNorm	-	-	-	20
	Fully-Connected4	-	-	-	2

size of 128.

- ResNet18 [10]: ResNet18 is a convolutional architecture adapted for analyzing time series by modifying input channels, leveraging residual blocks to capture temporal patterns.
- OFA [18]: OFA patches input sequence features, feeds them through a frozen GPT2 model with trainable positional embeddings and LayerNorm, and uses a final linear layer for classification.
- ADN18 [41]: ADN18 enhances CNN model with asymmetric convolutional kernels and attention mechanism to adaptively capture spatial-temporal features in spectrograms derived from Short-Time Fourier Transform.

3) *Evaluation Metrics*: In maritime target detection, achieving a high detection rate at an extremely low false alarm rate is imperative, as misinterpreting sea clutter as targets can have significant consequences, particularly in military operations. We evaluate the detection performance of different detectors at a false alarm rate of 0.005, considering our test set only comprises 6,000 clutter samples. Selecting a lower false alarm rate could result in unstable comparisons due to the limited number of clutter samples.

4) *Implementation Details*: The experimentally relevant hyperparameters and details are shown in Table II. For patching, the size of feature patches is set to 48. For the pre-trained LLM, the smallest version of GPT2 with  $F = 768$  feature dimension and the first  $L = 4$  layers of the GPT2 encoder are deployed. The network hyperparameters of the Autoencoder are shown in Table III. The value of  $\alpha$  in Eq.(22) is set to 0.9. All signal feature extraction operations are performed with MATLAB R2016a software. All network training experiments are conducted on a system equipped with an E5-2695v3 CPU, an NVIDIA 3090Ti GPU, and 64 GB of RAM.

TABLE IV  
DETECTION PERFORMANCE OF DIFFERENT METHODS WHEN THE FALSE ALARM RATE IS 0.005. THE BEST AND SECOND-BEST DETECTION RESULTS ARE HIGHLIGHTED IN RED AND BLUE, RESPECTIVELY.

Detector	HH	HV	VH	VV	AVG
RNN [14]	46.04	46.66	38.18	17.04	36.98
Bi-LSTM [14]	70.39	73.15	76.48	60.89	72.48
GRU [38]	76.46	77.55	73.96	67.48	73.86
Transformer [39]	52.95	71.73	67.32	55.67	61.92
PatchTST [40]	75.23	75.72	77.49	66.59	73.76
Resnet18 [10]	66.24	80.96	<b>82.31</b>	73.97	75.87
OFA [18]	74.19	80.38	79.71	70.36	76.16
ADN18 [41]	<b>79.74</b>	<b>83.50</b>	82.01	<b>78.02</b>	<b>80.82</b>
RadarLLM	<b>82.51</b>	<b>84.81</b>	<b>84.61</b>	<b>75.90</b>	<b>81.96</b>

### B. Comparison of Detection Performance, Speed, and Network Parameters Under Sufficient Training Samples

Table IV reports the detection rates achieved by RadarLLM and the eight baseline detectors introduced in Section IV-A2. All results are obtained with a fixed false alarm rate of 0.005 on the eight IPIX datasets. Compared to the best competing sequence feature detector, RadarLLM improves the detection rate by 7.60%, 3.85%, 2.30%, and 1.93% for the HH, HV, VH, and VV polarizations, respectively. Figure IV presents the complete ROC curves; it is evident that RadarLLM maintains the highest detection probability across the full range of false alarm rates. We also compare RadarLLM with ADN18, which relies on high-dimensional time–frequency maps and an enhanced CNN backbone. Despite using only compact sequence features, RadarLLM still delivers a 1.14% gain in

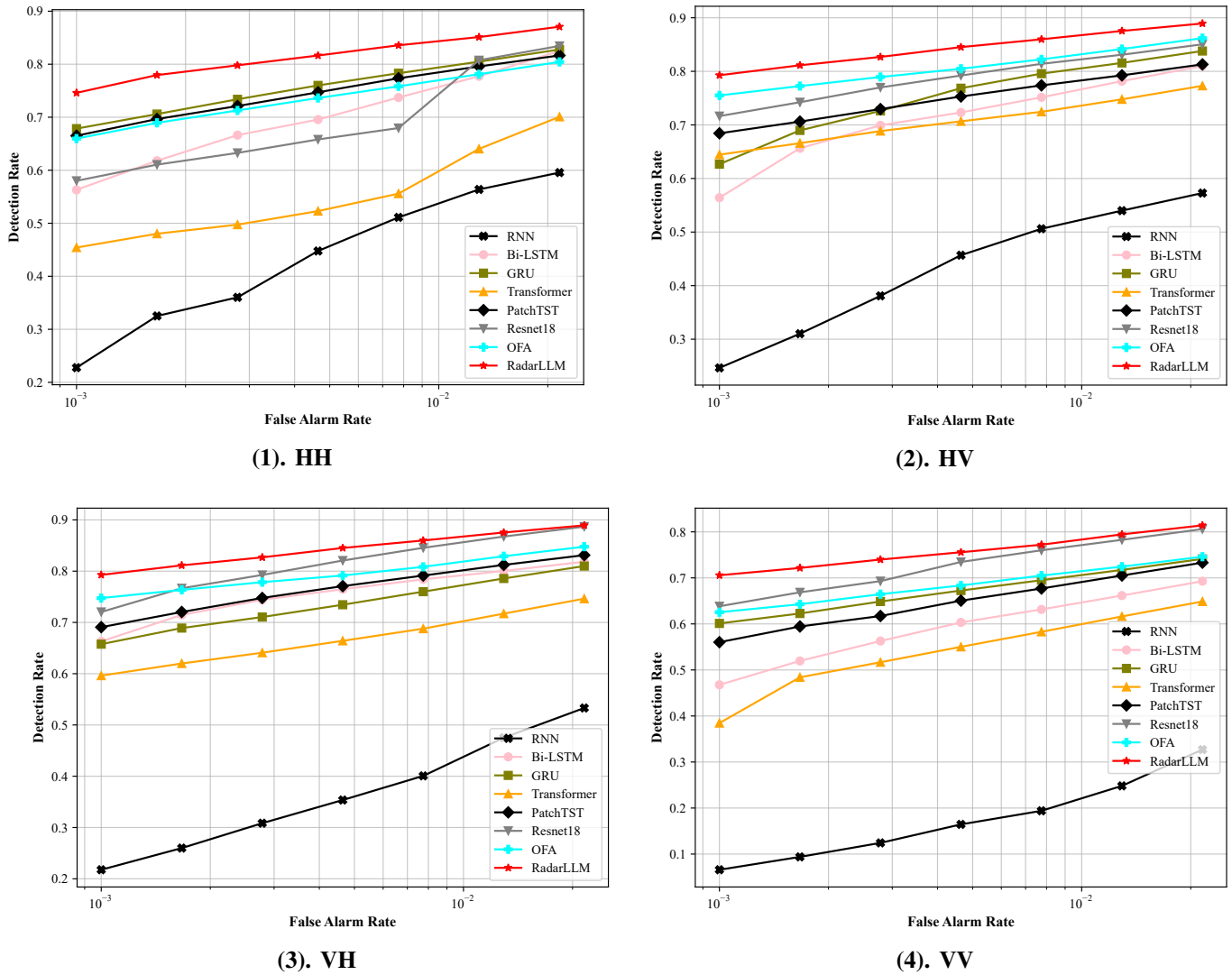


Fig. 7. Comparison of model detection performance on various datasets.

average detection rate.

Furthermore, we compare RadarLLM with other baseline models in terms of training complexity, total network parameters, and inference cost to evaluate its practicality for real-world deployment. The comparison results are summarized in Table V. Although RadarLLM has the highest total network parameters, the number of trainable parameters is comparable to those of other models, as the majority of its weights are frozen during fine-tuning. Notably, RadarLLM achieves an exceptionally low average inference latency. Specifically, it requires only 5.6561 seconds to process over 9,000 test samples, making it 28.44 times faster than the ADN18 method. This efficiency is primarily attributed to our patching strategy, which substantially reduces the number of feature tokens, and consequently, the computational overhead. Moreover, the intrinsic inference acceleration of the GPT architecture further enhances this performance gain. Together, these advantages make RadarLLM a promising solution for real-time marine target detection.

C. Comparison of Detection Performance Under Limited Training Samples With Baselines

Due to the inherent sparsity of radar targets in real-world scenarios, obtaining high-quality labeled samples for radar target detection presents a substantial challenge. Considering this issue, we conduct experiments under constrained training sample conditions to assess the effectiveness of RadarLLM. The samples are divided into three groups: (1) a training set using the first 10% of the observation time for both the target and clutter cells, (2) a validation set covering 10% to 15% of the observation time, and (3) a test set containing the remaining samples.

In Table VI, we report the detection performance of RadarLLM and several baseline methods under scenarios with limited training data. Compared with the experimental setup described in Section IV-A1, the advantages of RadarLLM become more pronounced. Specifically, RadarLLM achieves a substantial increase of **19.66%** in the average detection rate over the previously proposed sequence-feature based detector [14]. This marked improvement can be mainly attributed

TABLE V  
NETWORK PARAMETERS (TRAINING PARAMETERS/TOTAL PARAMETERS) AND INTERFERENCE TIME OF DIFFERENT METHODS.

Detector	Average interference time on one dataset(s)	Total network parameters(M)	Training network parameters(M)
RNN [14]	5.3587	0.0003	0.0003
Bi-LSTM [14]	5.6028	0.0016	0.0016
GRU [38]	5.7746	0.0008	0.0008
Transformer [39]	6.0678	0.0611	0.0611
PatchTST [40]	5.3727	0.0939	0.0939
Resnet18 [10]	5.4434	3.8454	3.8454
ADN18 [41]	160.9018	14.3315	14.3315
RadarLLM	5.6561	69.3932	2.4567

TABLE VI

DETECTION PERFORMANCE UNDER LIMITED TRAINING SAMPLES OF DIFFERENT METHODS WHEN THE FALSE ALARM RATE IS 0.005. THE BEST AND SECOND-BEST DETECTION RESULTS ARE HIGHLIGHTED IN RED AND BLUE, RESPECTIVELY.

Detector	HH	HV	VH	VV	AVG
RNN [14]	35.49	30.13	31.82	15.14	28.15
Bi-LSTM [14]	61.96	67.46	65.39	42.19	59.25
GRU [38]	70.43	74.14	74.20	59.47	69.56
Transformer [39]	70.22	64.56	65.31	51.15	62.81
PatchTST [40]	68.31	72.30	75.69	61.77	69.52
Resnet18 [10]	63.71	78.33	78.08	71.05	72.79
OFA [18]	73.64	76.81	77.44	63.33	72.81
ADN18 [41]	<b>75.45</b>	<b>81.50</b>	<b>80.81</b>	<b>70.97</b>	<b>77.18</b>
RadarLLM	<b>79.26</b>	<b>82.31</b>	<b>81.51</b>	<b>72.54</b>	<b>78.91</b>

to three key factors:

- First, leveraging pre-trained knowledge embedded in the large language model (LLM) provides RadarLLM with a beneficial parameter initialization, facilitating efficient optimization even when training data is limited. This prior knowledge significantly reduces the data dependency typical of conventional training strategies.
- Second, the substantial parameter scale of RadarLLM inherently grants robustness to distributional variations, enabling superior generalization compared to smaller-scale neural networks. Its extensive capacity allows it to capture complex data structures and efficiently handle variability across different radar detection scenarios.
- Third, the integration of a preference-aware loss function notably improves RadarLLM’s detection performance, especially in challenging scenarios characterized by low signal-to-clutter ratios (SCR).

#### D. Ablation Study

1) *Ablation Study on the Backbone Choice:* To validate the effectiveness of using pre-trained LLM, the ablation study is conducted in this section by removing or replacing the pre-trained LLM:

- 1) RadarLLM(0): In this variant, the pre-trained LLM is entirely removed, while all other components of the framework are kept unchanged.
- 2) RadarLLM(T): In this variant, the pre-trained LLM is replaced with a randomly initialized transformer block.
- 3) RadarLLM(R): In this variant, the network architecture and fine-tuning procedure of the original LLM are maintained, but its pre-trained parameters are replaced with random initialization.

In Table VII, we show the results of the ablation study. It can be seen that the removal or exchange of pre-trained LLM results in notable performance degradation, indicating the necessity of pretrained LLM for high detection performance.

2) *Ablation Study on the Loss Function:* In addition, we compare the fine-tuning effects of preference-aware loss and CE loss on low SCR datasets. First, to facilitate a direct and quantitative comparison between the two loss functions, we aggregate the outputs of all feature tokens by applying a softmax normalization function followed by averaging operation. The resulting probabilities are then used for target detection. In Fig. 9, we evaluate the detection rate on the test samples of different low SCR datasets at different training epochs. It can be seen that preference-aware loss achieves an improvement of around **1%-15%** compared to cross-entropy loss (uniformly optimized on all feature patches) in different training epochs and datasets. In Table VIII, we show the detection performance of the reference model. It can be seen that the optimal detection performance of the fine-tuned model outperforms the reference model by approximately **3%-18%** across various datasets. Notably, despite this remarkably significant performance gap, leveraging the reference model to score individual feature tokens still yields significant performance gains.

Although the preceding results are promising, a direct comparison between the proposed preference-aware (PA) loss and the conventional end to end cross-entropy (CE) loss remains lacking. To bridge this gap, we evaluate multiple model variants: RadarLLM(PA) vs. RadarLLM(CE), and PatchTST(PA) vs. PatchTST(CE). Models labeled with (PA) adopt the proposed token-level reweighting strategy based on learning value, while those with (CE) rely on standard cross-entropy loss. For further comparison, we include a sample-level reweighting baseline, denoted as WCE [28], where training weights are adjusted at the sample level.

As summarized in Table IX, the PA loss consistently yields superior performance across all datasets, especially under low SCR conditions. For instance, RadarLLM(PA) achieves an average gain of **9.9%** over RadarLLM(CE), while PatchTST(PA) improves by **7.0%** over its CE-based counterpart. Notably, token-level reweighting in both PA variants outperforms WCE, highlighting the advantage of fine-grained reweighting in enhancing detection under challenging scenarios.

#### E. Analysis of the Effect of Hyperparameters on Experimental Results

We first investigate the impact of patch size on RadarLLM’s performance. The results of the ablation study are summarized

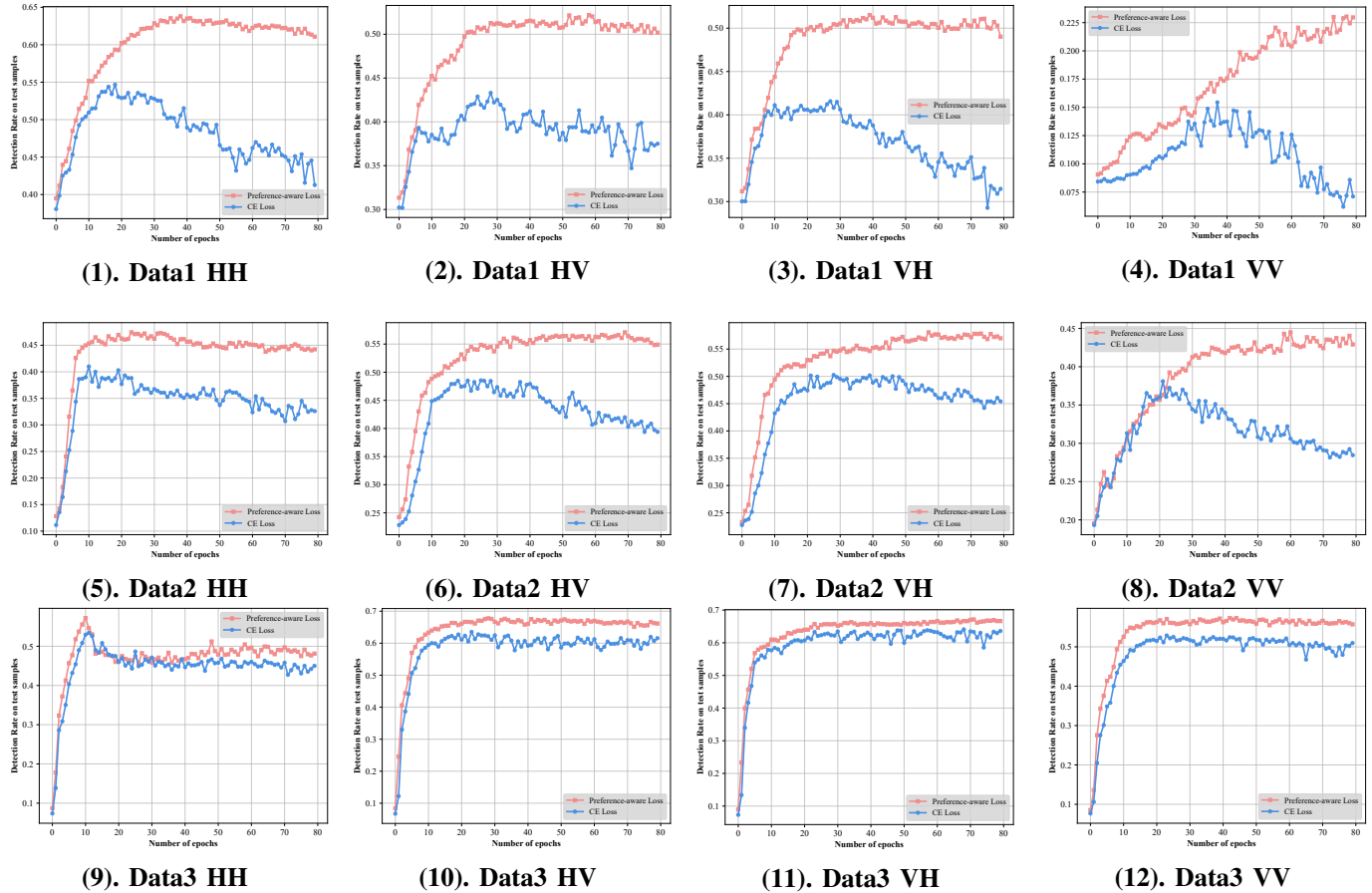


Fig. 8. Comparison of cross-entropy loss and preference-aware loss on low SCR datasets. We compare detection rates across different datasets and epochs, highlighting the improvements achieved by the preference-aware loss function.

TABLE VII  
RESULTS OF ABLATION STUDY ON THE BACKBONE CHOICE.

	HH	HV	VH	VV	AVG
RadarLLM	<b>82.71</b>	<b>83.84</b>	<b>83.91</b>	<b>75.23</b>	<b>81.42</b>
RadarLLM(0)	77.51	79.38	80.35	69.97	76.80
RadarLLM(T)	78.25	79.77	81.16	72.13	77.83
RadarLLM(R)	75.19	75.44	75.81	65.15	72.90

TABLE VIII  
DETECTION PERFORMANCE OF REFERENCE MODEL ON THREE LOW SCR DATASETS.

Reference model	HH	HV	VH	VV
Data1	46.68	45.21	46.75	18.48
Data2	34.87	50.75	48.41	42.51
Data3	47.39	59.82	61.85	44.72

TABLE IX  
RESULTS OF ABLATION STUDY ON THE LOSS FUNCTION.

	Data1	Data2	Data3	AVG
RadarLLM(PA)	<b>52.06(+16.8)</b>	<b>54.87(+5.4)</b>	<b>65.81(+7.5)</b>	<b>57.58(+9.9)</b>
RadarLLM(WCE)	43.51(+8.8)	53.95(+4.9)	64.55(+6.8)	54.84(+7.7)
RadarLLM(CE)	34.73	48.96	57.80	47.16
PatchTST(PA)	47.48(+8.1)	50.29(+5.9)	62.42(+7.0)	53.40(+7.0)
PatchTST(WCE)	46.68(+7.8)	48.96(+5.0)	57.80(+2.9)	51.15(+5.2)
PatchTST(CE)	38.91	43.92	54.89	45.91

TABLE X  
THE AVERAGE DETECTION RATE, INTERFERE TIME ON ONE DATASET, AND TOTAL/TRAINING NETWORK PARAMETERS OF RADARGPT WITH DIFFERENT NUMBER OF PATCH SIZE.)

	Average DR	Average IT(s)
RadarLLM(with a patch size of 32)	79.44	5.9259
RadarLLM(with a patch size of 48)	81.96	5.6561
RadarLLM(with a patch size of 64)	79.09	5.6222

in Table X. Using a patch size of 48 achieves the highest detection rate, outperforming configurations with smaller (32) and larger (64) patch sizes. These results highlight the importance of selecting an appropriate patch size to optimize the performance of RadarLLM.

We then investigate the impact of the number of GPT2 layers on RadarLLM’s performance. Our ablation study on GPT2 layer configurations is presented in Table XI. Activating four GPT2 layers achieves the highest detection rate, outperforming both shallower configurations and deeper ones. These results highlight two key observations: (1) a model with insufficient layers fails to fully leverage the cross-modal transfer capabilities of the language model, while excess layers suffer from overfitting due to the task-irrelevant network parameters in deeper layers. (2) Although utilizing more GPT2 layers significantly increases the scale of model parameters, the impact on inference latency is minimal. Specifically, the

TABLE XI

THE AVERAGE DETECTION RATE, INTERFERE TIME ON ONE DATASET, AND TOTAL/TRAINING NETWORK PARAMETERS OF RADARLLM WITH DIFFERENT NUMBER OF GPT2 LAYERS. (RADARLLM(N) REPRESENTS RADARLLM WITH N LLM LAYERS.)

	Average DR	Average IT(s)	Total/Training NP(M)
RadarLLM(0)	77.41	5.3484	41.0410/2.4445
RadarLLM(2)	81.29	5.4812	55.2175/2.4506
RadarLLM(4)	81.96	5.6561	69.3932/2.4567
RadarLLM(6)	80.42	5.7331	83.5690/2.4628
RadarLLM(8)	80.01	5.8655	97.7447/2.4690

inference speed of GPT2(8) remains approximately 91% of that of GPT2(0), as the inherent inference acceleration of the GPT architecture mitigates the computational overhead introduced by deeper layers.

#### F. Case Study of the Effectiveness of Feature Token Importance

To further demonstrate the effectiveness of the proposed preference-aware loss function, we conduct a case study analyzing the training weight dynamics of feature tokens for two representative sequence features: Short-Time Fourier Transform Magnitude Spectrum (SMS) and Instantaneous Phase (IP) features.

The SMS feature exhibits a distinctive rise and fall pattern indicative of target presence, primarily characterized by feature tokens 26 and 27. As illustrated in Fig. 9, these tokens initially receive high attention weights during training, underscoring the model’s emphasis on learning these salient patterns. However, as training progresses, the model rapidly assimilates these features, resulting in a marked decline in their weights after approximately 10 epochs. This adaptive behavior reflects the model’s ability to dynamically reallocate attention from well-learned patterns to more complex or informative features, thus mitigating the risk of overfitting to easily recognizable signal features.

In contrast, the IP feature demonstrates a more complex structure, encompassing both moderately varying patterns associated with target echos (corresponding to tokens 0, 3, and 4) and rapidly fluctuating patterns caused by clutter-induced noise (corresponding to tokens 8, 9, and 10). These six tokens, arranged from left to right, align with the gray-lighted segments in the IP feature map illustrated in Fig. 9. During training, tokens 0, 3, and 4 consistently receive elevated attention weights, typically exceeding 1, indicating the model’s sustained emphasis on these informative yet challenging-to-learn feature tokens. In contrast, tokens 8, 9, and 10 are assigned substantially lower weights, which highlights the model’s ability to suppress excessive learning from noisy and less informative feature tokens.

## V. CONCLUSION AND FUTURE WORK

In this study, we propose RadarLLM, a novel framework that integrates a pre-trained LLM with a lightweight reference model for small marine target detection. Employing LoRA adaptation and preference-aware loss, we selectively optimize different feature patches according to their learning values

in a lightweight form, effectively reducing model overfitting in low SCR environments. Extensive experimental results demonstrate that RadarLLM significantly outperforms state-of-the-art baselines across sufficient training data, and limited training data settings in various detection scenarios. These results highlight the considerable potential of LLMs in radar signal processing, especially for challenging small marine target detection. Looking ahead, several promising research directions emerge:

- 1) Future studies should investigate the use of more sophisticated open-source pre-trained LLMs, such as Meta’s LLaMA2 or LLaMA3 [42]. These much larger models may offer enhanced parameter transfer capabilities compared to GPT2.
- 2) Although the present approach demonstrates the effectiveness of the selected reference model, there remains considerable potential to explore alternative architectures. Future investigations could examine models such as Mamba [43] or leverage iterative training frameworks, which may further enhance the performance and training efficiency of the reference model.
- 3) To address the storage demands of using large language models (LLMs), we suggest employing model compression strategies, including quantization, pruning, and knowledge distillation. These methods aim to reduce model size while maintaining performance, facilitating the deployment of LLMs in resource-constrained environments.

## REFERENCES

- [1] X. Chen, J. Guan, Z. Bao, and Y. He, “Detection and extraction of target with micromotion in spiky sea clutter via short-time fractional fourier transform,” *IEEE Transactions on Geoscience and Remote Sensing*, vol. 52, no. 2, pp. 1002–1018, 2013.
- [2] P.-L. Shui, D.-C. Li, and S.-W. Xu, “Tri-feature-based detection of floating small targets in sea clutter,” *IEEE Transactions on Aerospace and Electronic Systems*, vol. 50, no. 2, pp. 1416–1430, 2014.
- [3] S.-N. Shi and P.-L. Shui, “Sea-surface floating small target detection by one-class classifier in time-frequency feature space,” *IEEE Transactions on Geoscience and Remote Sensing*, vol. 56, no. 11, pp. 6395–6411, 2018.
- [4] X. Bai, S. Xu, J. Zhu, Z. Guo, and P. Shui, “Floating small target detection in sea clutter based on multifeature angle variance,” *IEEE Journal of Selected Topics in Applied Earth Observations and Remote Sensing*, vol. 16, pp. 9422–9436, 2023.
- [5] W. Zhao, M. Jin, G. Cui, and Y. Wang, “Eigenvalues-based detector design for radar small floating target detection in sea clutter,” *IEEE Geoscience and Remote Sensing Letters*, vol. 19, pp. 1–5, 2021.
- [6] S. Xu, J. Zhu, J. Jiang, and P. Shui, “Sea-surface floating small target detection by multifeature detector based on isolation forest,” *IEEE Journal of Selected Topics in Applied Earth Observations and Remote Sensing*, vol. 14, pp. 704–715, 2020.
- [7] X. Chen, N. Su, Y. Huang, and J. Guan, “False-alarm-controllable radar detection for marine target based on multi features fusion via cnns,” *IEEE Sensors Journal*, vol. 21, no. 7, pp. 9099–9111, 2021.
- [8] Q. Qu, Y.-L. Wang, W. Liu, and B. Li, “A false alarm controllable detection method based on cnn for sea-surface small targets,” *IEEE Geoscience and Remote Sensing Letters*, vol. 19, pp. 1–5, 2022.
- [9] S. Xu, H. Ru, D. Li, P. Shui, and J. Xue, “Marine radar small target classification based on block-whitened time–frequency spectrogram and pre-trained cnn,” *IEEE Transactions on Geoscience and Remote Sensing*, vol. 61, pp. 1–11, 2023.
- [10] S. Xia, Y. Kong, K. Xiong, and G. Cui, “Target detection in sea clutter via contrastive learning,” *IEEE Transactions on Instrumentation and Measurement*, vol. 72, pp. 1–13, 2023.

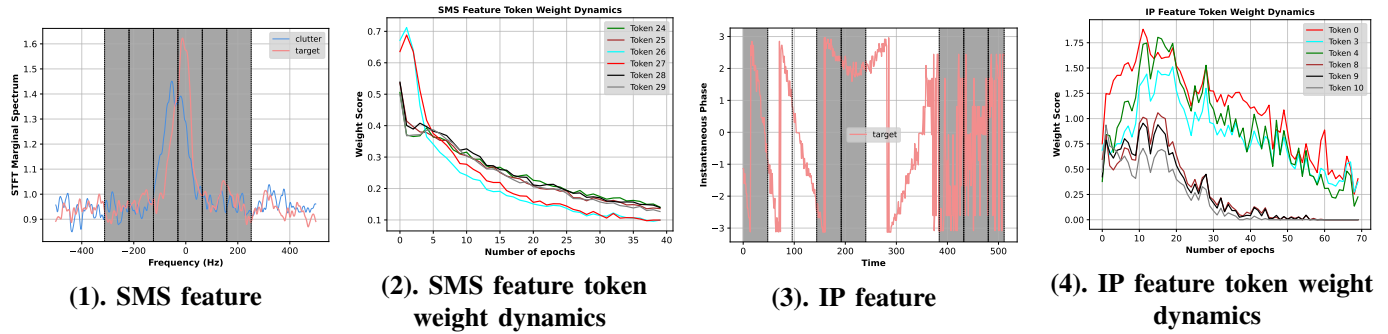


Fig. 9. Dynamics of feature token weights during training: (a) SMS feature token weight dynamics, (b) IP feature token weight dynamics. The graphs show how the attention weights assigned to individual feature tokens evolve over epochs, emphasizing the model’s ability to adaptively focus on informative features and suppress noisy tokens.

- [11] Y. Wang, W. Zhao, X. Wang, J. Chen, H. Li, and G. Cui, “Nonhomogeneous sea clutter suppression using complex-valued u-net model,” *IEEE Geoscience and Remote Sensing Letters*, vol. 19, pp. 1–5, 2022.
- [12] J. Wang and S. Li, “Maritime radar target detection in sea clutter based on cnn with dual-perspective attention,” *IEEE Geoscience and Remote Sensing Letters*, vol. 20, pp. 1–5, 2022.
- [13] J.-Y. Li, X.-J. Zhang, Z.-J. Zhao, P.-L. Shui, and S.-W. Xu, “Small target classification of maritime radars using standardized time-frequency distribution images and residual networks with improved focal loss,” *IEEE Transactions on Instrumentation and Measurement*, vol. 74, pp. 1–17, 2025.
- [14] H. Wan, X. Tian, J. Liang, and X. Shen, “Sequence-feature detection of small targets in sea clutter based on bi-ilstm,” *IEEE Transactions on Geoscience and Remote Sensing*, vol. 60, pp. 1–11, 2022.
- [15] N. Su, X. Chen, J. Guan, and Y. Huang, “Maritime target detection based on radar graph data and graph convolutional network,” *IEEE Geoscience and Remote Sensing Letters*, vol. 19, pp. 1–5, 2021.
- [16] H. Ru, S. Xu, Q. He, and P. Shui, “Marine small floating target detection method based on fusion weight and graph dynamic attention mechanism,” *IEEE Transactions on Geoscience and Remote Sensing*, vol. 61, pp. 1–11, 2023.
- [17] N. Su, X. Chen, J. Guan, Y. Huang, X. Wang, and Y. Xue, “Radar maritime target detection via spatial-temporal feature attention graph convolutional network,” *IEEE Transactions on Geoscience and Remote Sensing*, vol. 62, pp. 1–15, 2024.
- [18] T. Zhou, P. Niu, L. Sun, R. Jin *et al.*, “One fits all: Power general time series analysis by pretrained lm,” *Advances in neural information processing systems*, vol. 36, pp. 43 322–43 355, 2023.
- [19] X. Liu, J. Hu, Y. Li, S. Diao, Y. Liang, B. Hooi, and R. Zimmermann, “Unitime: A language-empowered unified model for cross-domain time series forecasting,” in *Proceedings of the ACM on Web Conference 2024*, 2024, pp. 4095–4106.
- [20] M. Jin, S. Wang, L. Ma, Z. Chu, J. Y. Zhang, X. Shi, P.-Y. Chen, Y. Liang, Y.-F. Li, S. Pan *et al.*, “Time-llm: Time series forecasting by re-programming large language models,” *arXiv preprint arXiv:2310.01728*, 2023.
- [21] T. Zheng and L. Dai, “Large language model enabled multi-task physical layer network,” *arXiv preprint arXiv:2412.20772*, 2024.
- [22] Z. Xu, T. Zheng, and L. Dai, “Llm-empowered near-field communications for low-altitude economy,” *IEEE Transactions on Communications*, pp. 1–1, 2025.
- [23] Z. Li, Q. Yang, Z. Xiong, Z. Shi, and T. Q. Quek, “Bridging the modality gap: Enhancing channel prediction with semantically aligned llms and knowledge distillation,” *arXiv preprint arXiv:2505.12729*, 2025.
- [24] B. Liu, X. Liu, S. Gao, X. Cheng, and L. Yang, “Llm4cp: Adapting large language models for channel prediction,” *Journal of Communications and Information Networks*, vol. 9, no. 2, pp. 113–125, 2024.
- [25] Q. Hu, L. Zhang, X. Wang, G. Li, Y. Liu, and X.-P. Zhang, “When marine radar target detection meets pretrained large language models,” in *IGARSS 2025-2025 IEEE International Geoscience and Remote Sensing Symposium*, 2025, in press.
- [26] E. J. Hu, Y. Shen, P. Wallis, Z. Allen-Zhu, Y. Li, S. Wang, L. Wang, W. Chen *et al.*, “Lora: Low-rank adaptation of large language models,” *ICLR*, vol. 1, no. 2, p. 3, 2022.
- [27] Z. Lin, Z. Gou, Y. Gong, X. Liu, Y. Shen, R. Xu, C. Lin, Y. Yang, J. Jiao, N. Duan *et al.*, “Rho-1: Not all tokens are what you need,” *arXiv preprint arXiv:2404.07965*, 2024.
- [28] S. Mindermann, J. M. Brauner, M. T. Razzak, M. Sharma, A. Kirsch, W. Xu, B. Höltingen, A. N. Gomez, A. Morisot, S. Farquhar *et al.*, “Prioritized training on points that are learnable, worth learning, and not yet learnt,” in *International Conference on Machine Learning*. PMLR, 2022, pp. 15 630–15 649.
- [29] J. Wang and S. Li, “Maritime radar target detection model self-evolution based on semisupervised learning,” *IEEE Transactions on Geoscience and Remote Sensing*, vol. 62, pp. 1–11, 2023.
- [30] Y. Wang, X. Chen, X. Wang, C. Zang, W. Zhao, and G. Cui, “Radar detection self-evolution based on incremental learning in time-varying clutter environments,” *IEEE Transactions on Instrumentation and Measurement*, vol. 73, pp. 1–13, 2024.
- [31] Y. Chang, X. Wang, J. Wang, Y. Wu, L. Yang, K. Zhu, H. Chen, X. Yi, C. Wang, Y. Wang *et al.*, “A survey on evaluation of large language models,” *ACM transactions on intelligent systems and technology*, vol. 15, no. 3, pp. 1–45, 2024.
- [32] A. Radford, J. Wu, R. Child, D. Luan, D. Amodei, I. Sutskever *et al.*, “Language models are unsupervised multitask learners,” *OpenAI blog*, vol. 1, no. 8, p. 9, 2019.
- [33] Y. Sheng, K. Huang, L. Liang, P. Liu, S. Jin, and G. Y. Li, “Beam prediction based on large language models,” *arXiv preprint arXiv:2408.08707*, 2024.
- [34] T. An, Y. Zhou, H. Zou, and J. Yang, “Iot-llm: Enhancing real-world iot task reasoning with large language models,” *arXiv preprint arXiv:2410.02429*, 2024.
- [35] H. Xu, L. Han, Q. Yang, M. Li, and M. Srivastava, “Penetrative ai: Making llms comprehend the physical world,” in *Proceedings of the 25th International Workshop on Mobile Computing Systems and Applications*, 2024, pp. 1–7.
- [36] M. Tan, M. Merrill, V. Gupta, T. Althoff, and T. Hartvigsen, “Are language models actually useful for time series forecasting?” *Advances in Neural Information Processing Systems*, vol. 37, pp. 60 162–60 191, 2024.
- [37] A. Kendall, Y. Gal, and R. Cipolla, “Multi-task learning using uncertainty to weigh losses for scene geometry and semantics,” in *Proceedings of the IEEE conference on computer vision and pattern recognition*, 2018, pp. 7482–7491.
- [38] K. Cho, “Learning phrase representations using rnn encoder-decoder for statistical machine translation,” *arXiv preprint arXiv:1406.1078*, 2014.
- [39] A. Vaswani, N. Shazeer, N. Parmar, J. Uszkoreit, L. Jones, A. N. Gomez, L. Kaiser, and I. Polosukhin, “Attention is all you need,” *arXiv preprint arXiv:1706.03762*, 2017.
- [40] Y. Nie, N. H. Nguyen, P. Sinthong, and J. Kalagnanam, “A time series is worth 64 words: Long-term forecasting with transformers,” *arXiv preprint arXiv:2211.14730*, 2022.
- [41] Q. Qu, W. Liu, J. Wang, B. Li, N. Liu, and Y.-L. Wang, “Enhanced cnn-based small target detection in sea clutter with controllable false alarm,” *IEEE Sensors Journal*, vol. 23, no. 9, pp. 10 193–10 205, 2023.
- [42] H. Touvron, T. Lavril, G. Izacard, X. Martinet, M.-A. Lachaux, T. Lacroix, B. Rozière, N. Goyal, E. Hambro, F. Azhar *et al.*, “Llama: Open and efficient foundation language models,” *arXiv preprint arXiv:2302.13971*, 2023.

- [43] A. Gu and T. Dao, “Mamba: Linear-time sequence modeling with selective state spaces,” *arXiv preprint arXiv:2312.00752*, 2023.